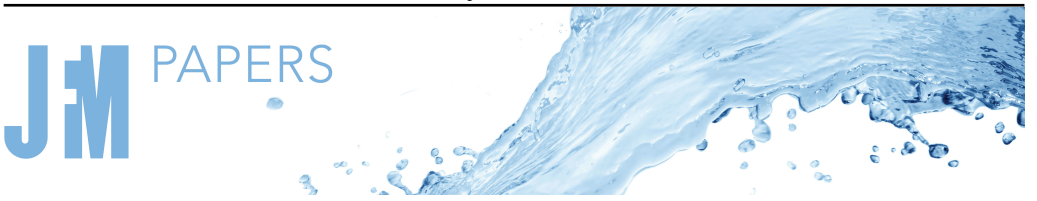
J. Fluid Mech. (2026), *vol.* 1036, A55, doi:10.1017/jfm.2026.11664



Capillary currents and viscous droplet spreading

David Darrow[1], **Lucas Warwaruk**[2] **and John W.M. Bush**[1]

[1]Department of Mathematics, Massachusetts Institute of Technology, Cambridge, MA 02139, USA

[2]Department of Mechanical Engineering, Massachusetts Institute of Technology, Cambridge, MA 02139, USA

Corresponding authors: David Darrow, ddarrow@mit.edu; John W.M. Bush, bush@math.mit.edu

(Received 10 August 2025 UTC; revised 13 March 2026 UTC; accepted 8 May 2026 UTC)

We present the results of a combined experimental and theoretical study of the spreading of viscous droplets over rigid substrates. First, we experimentally investigate the wetting of a roughened glass surface by a viscous droplet of silicone oil, wide and shallow relative to the capillary length ℓ_c. The horizontal radius of the droplet grows according to an $R_{drop} \sim t^{1/8}$ scaling, reminiscent of viscous gravity currents (Lopez *et al.* 1976 *J. Colloid Interface Sci.*, vol. 56, pp. 460–468). The droplet is preceded by a mesoscopic fluid film that percolates through the rough substrate, its radius increasing according to $R_{film} \sim t^{3/8}/(\log t)^{1/2}$. To rationalise these observed scalings, we develop a new 'capillary current' model for the spreading of shallow droplets with arbitrary radius on rough surfaces. Furthermore, on the basis of established similarities between droplet spreading over wetted rough and smooth substrates (Cazabat & Cohen Stuart, 1986 *J. Phys. Chem.*, vol. 90, pp. 5845–5845), we argue its relevance to a broader class of spreading problems. We propose that, throughout their evolution, shallow droplets maintain a quasi-equilibrium balance between hydrostatic and curvature pressure, perturbed only by unbalanced contact line forces arising along the droplet's edge. For drops with horizontal radii small with respect to ℓ_c, our model converges to the original description of Hervet & de Gennes (1984 *C. R. Acad. Sci. II*, vol. 299, pp. 499–503) and thereby recovers the classic spreading laws of Hoffman (1975 *J. Colloid Interface Sci.*, vol. 50, pp. 228–241), Voinov (1976 *Fluid Dyn.*, vol. 11, pp. 714–721) and Tanner (1979 *J. Phys. D: Appl. Phys.* vol. 12, p. 1473). For drops wide with respect to ℓ_c, it rationalises why millimetric, surface-tension-driven capillary currents exhibit the same spreading behaviour as relatively large-scale viscous gravity currents.

Key words: capillary flows, wetting and wicking, drops

1. Introduction

A volume of liquid placed onto a solid substrate will spread in response to gravitational and interfacial forces, with its spreading resisted by a combination of inertial and viscous

© The Author(s), 2026. Published by Cambridge University Press.

https://doi.org/10.1017/jfm.2026.11664 Published online by Cambridge University Press

stresses. The relative importance of these four effects is prescribed by the Bond number $Bo = \rho g h^2/\sigma$ and the Reynolds number $Re = \rho U h/\mu$. Here, σ is the surface tension at the air–liquid interface, ρ and μ are the liquid's density and dynamic viscosity, h is its maximum depth, U is its characteristic speed and g is the acceleration due to gravity. While our work primarily focuses on the spreading of viscous, shallow droplets ($Re \ll 1$, $Bo \lesssim 1$), it is helpful to first discuss the relatively well-established theory of viscous gravity currents ($Re \ll 1$, $Bo \gg 1$).

If $Re \ll 1$ and $Bo \gg 1$, corresponding to a deep, viscous volume of liquid, then the fluid spreads out in the form of a viscous gravity current (Simpson 1999; Huppert 2006; Ungarish 2009). Suppose it has a horizontal radius R and characteristic volume $V \sim hR^2$. Gravity creates an overpressure $\rho g h$ in the centre of the volume, and thus a horizontal pressure gradient $\rho g h/R$ that drives the fluid outward. This force is balanced by a viscous stress $\mu \dot{R}/h^2$, yielding the classic scaling (Huppert 1982)

$$\dot{R} \sim \frac{\rho g}{\mu}\frac{h^3}{R} \sim \frac{\rho g}{\mu}\frac{V^3}{R^7}, \qquad R \sim V^{3/8} t^{1/8}. \tag{1.1}$$

This gravity–viscosity balance is known to drive a number of macroscopic flows in nature and industry, including creeping lava flows, molten glass flows in the production of sheet glass and honey spreading over toast (Huppert 2006).

The scaling (1.1) holds until the depth h becomes comparable to the capillary length $\ell_c = (\sigma/\rho g)^{1/2}$, at which point one expects interfacial effects to become important. Perhaps surprisingly, the scaling $R \sim V^{3/8} t^{1/8}$ does not change when a wide droplet enters this latter regime, specifically when $h \lesssim \ell_c$ and $R \gg \ell_c$ (Bonn *et al.* 2009). Lopez, Miller & Ruckenstein (1976) proposed that wide, shallow droplets behave similarly to deeper gravity currents – namely, that spreading is driven by gravitational overpressure and resisted by energy dissipation throughout the droplet bulk. Subsequent work of Ehrhard & Davis (1991) offered an alternate, edge-localised form of the energy dissipation, and Voinov (1995, 1999) suggested perturbatively incorporating the effect of surface tension on the droplet edge. Even still, the basic physical picture of gravity-driven motion in this small-Bond-number regime remains widely accepted (Bonn *et al.* 2009; Popescu *et al.* 2012).

In the present work, we propose an alternative perspective on the spreading of wide drops. First, we experimentally investigate the spreading of a wide, shallow drop of silicone oil over a roughened glass surface. Silicone oil is totally wetting with respect to borosilicate glass, so the drop exhibits a wet Cassie state (de Gennes, Brochard-Wyart & Quere 2003), in which a thin film of liquid percolates through the rough substrate ahead of the drop's advancing edge. We refer to such a film as a 'Darcy precursor film' in order to distinguish it from the microscopic precursor films that appear on smooth substrates (Hardy 1919). As first established by Cazabat & Cohen Stuart (1986), the similarities between Darcy and microscopic films serve to create strong dynamical similarities between the total wetting of rough and smooth substrates. In our case, we observe that the horizontal droplet radius R_1 grows according to $R_1 \sim t^{1/8}$, consistent with existing literature, but the radius R_2 of the thin film closely adheres to a new scaling $R_2 \sim t^{3/8}/(\log t)^{1/2}$.

To rationalise these findings, we develop a new 'capillary current' model for the spreading of shallow, viscous droplets, with horizontal radius either small or large with respect to ℓ_c, over either rough or smooth substrates. In short, we propose that such a droplet maintains a quasi-equilibrium balance between hydrostatic and curvature pressure, perturbed only by unbalanced contact line forces along its edge. Our proposed model

https://doi.org/10.1017/jfm.2026.11664 Published online by Cambridge University Press

converges to the original description of Hervet & de Gennes (1984) in the small-droplet limit ($R_1 \ll \ell_c$), thereby recovering the classic scalings of Hoffman (1975), Voinov (1976) and Tanner (1979). Namely, in the small-droplet limit, the droplet retains the shape of a spherical cap, and the droplet radius R_1, volume V and apparent contact angle θ satisfy

$$\dot{R}_1 \sim \theta^3, \qquad R_1 \sim V^{3/10} t^{1/10}. \tag{1.2}$$

In the large-droplet limit ($R_1 \gg \ell_c$), our model offers a self-consistent rationale for the $R_1 \sim V^{3/8} t^{1/8}$ scaling first observed by Lopez *et al.* (1976), and clarifies the nature of the small-to-large-droplet transition observed by Cazabat & Cohen Stuart (1986) and Ehrhard (1993). In addition to our own experimental results for large drops on rough substrates, our model rationalises the data of Dorbolo (2021) for the spreading of Darcy precursor films ahead of small droplets, and the data of Cazabat & Cohen Stuart (1986) for the small-to-large-droplet transition over smooth substrates. Our model also extends naturally to the case of partial wetting, where it reproduces the predictions of de Ruijter, De Coninck & Oshanin (1999) and Durian *et al.* (2022) for the early-time spreading behaviour of partially wetting drops. Taken together, our study suggests commonalities between large and small drops spreading over both rough and smooth substrates, under conditions of both total and partial wetting.

We present the basic physical picture of viscous droplet spreading in § 2, where we also provide a brief review of relevant literature. In § 3, we present our own experimental results on the spreading of large drops of silicone oil over roughened glass. We introduce our theoretical model in § 4 in order to rationalise the observed spreading behaviour. In § 5, we discuss the broader relevance of our model, which suggests a new perspective on the experiments of Cazabat & Cohen Stuart (1986), de Ruijter *et al.* (1999) and Dorbolo (2021). We propose additional experiments and directions of further study in § 6.

2. Physical picture

When a liquid droplet is placed on a rigid substrate, its evolution depends on several geometric and chemical factors. Of central importance are (i) whether spreading is resisted by viscosity or inertia, (ii) whether the drop is shallow, deep, narrow or wide with respect to the capillary length $\ell_c = (\sigma/\rho g)^{1/2}$, (iii) whether the drop totally or partially wets the substrate and (iv) whether the substrate itself is rough or smooth. We focus here on the case of shallow, viscous drops, for which

$$Bo = \rho g h^2/\sigma \lesssim 1, \qquad Re = \rho U h/\mu \ll 1. \tag{2.1}$$

Within this regime, we consider both 'small' ($R \ll \ell_c$) and 'large' ($R \gg \ell_c$) drops, and both smooth and rough substrates. In the latter case, we assume the roughness scale h_2 of the substrate is small relative to the droplet depth: $h_2 \ll h \lesssim \ell_c$.

For one, the extent to which the liquid wets the substrate is strongly influenced by surface chemistry. Indeed, if γ_{sl} and γ_{sv} are the solid–liquid and solid–vapour interfacial tensions, respectively, the regimes of total wetting and partial wetting can be distinguished by the spreading parameter

$$S = \gamma_{sv} - \gamma_{sl} - \sigma. \tag{2.2}$$

If $S < 0$, then the droplet partially wets the substrate, and will spread until reaching a static equilibrium marked by an equilibrium contact angle $\theta_{eq} > 0$. In this case, the horizontal force balance at the contact line yields Young's law,

$$\sigma \cos\theta_{eq} + \gamma_{sl} = \gamma_{sv} \qquad \Longrightarrow \qquad \cos\theta_{eq} = 1 + S/\sigma, \tag{2.3}$$

https://doi.org/10.1017/jfm.2026.11664 Published online by Cambridge University Press

which ensures $\theta_{eq} > 0$ provided that $S < 0$. Alternatively, if $S > 0$, then no such balance is possible, and the droplet totally wets the substrate: the drop spreads until its depth becomes comparable to the roughness scale of a rough substrate, or the molecular scale for a smooth substrate. We note that this physical picture can be further complicated if, for example, the liquid is volatile or the substrate has deep, porous structure. While such issues are beyond the scope of our study, we direct the reader to Bonn *et al.* (2009), Popescu *et al.* (2012) and Gambaryan-Roisman (2014) for reviews of a broader class of spreading problems.

We primarily focus on the case of total wetting, for which $S > 0$, though we return to the question of partial wetting in § 5. A drop totally wetting a rough substrate gives rise to a 'Darcy precursor film' of liquid that percolates ahead of the drop's advancing edge (de Gennes *et al.* 2003), with depth comparable to the roughness scale h_2 (figure 1*e*). Notably, a similar physical picture holds for smooth substrates: it was discovered by Hardy (1919) that the total wetting of a smooth substrate is accompanied by the formation of a microscopic precursor film that extends ahead of the visible droplet (figure 1*d*). In both cases, the drop spreads over a liquid layer, never coming in direct contact with the solid. The presence of the precursor film on a smooth substrate provides a resolution to the classic paradox of contact line motion (Huh & Scriven 1971; de Gennes 1985; Joanny & de Gennes 1986).

We discuss the leading-order geometry of the droplet in § 2.1, review the existing models for viscous droplet spreading in §§ 2.2–2.4, and review the existing model for the spreading of Darcy precursor films in § 2.5. A theoretical model that revises both physical pictures (i.e. for both droplet and film spreading) will be introduced in § 4. We do not treat the spreading of microscopic precursor films in the present work, but refer the reader to the reviews of Bonn *et al.* (2009) and Popescu *et al.* (2012) for a detailed discussion of the topic.

2.1. *Quasi-equilibrium geometry*

The basic geometry of our system is depicted in figure 1. We suppose for simplicity that the apparent contact angle θ satisfies $\theta \lesssim \pi/4$ (so that $\sin\theta \approx \tan\theta \approx \theta$) and that the droplet is axisymmetric. Here and below, we fix non-dimensionalised units such that

$$\frac{\sigma}{\rho g} = \frac{\sigma}{\mu} = 1, \qquad p_{atm.} = 0. \tag{2.4}$$

Equivalently, we non-dimensionalise by the length, velocity and time scales

$$\ell_c = \sqrt{\sigma/\rho g}, \qquad u_c = \sigma/\mu, \qquad \tau_c = \ell_c/u_c, \tag{2.5}$$

and we tare the pressure such that $p_{atm.} = 0$.

To a good approximation, after a momentary equilibration period when the droplet is first placed on a substrate (Biance, Clanet & Quéré 2004; Eddi, Winkels & Snoeijer 2013), the instantaneous droplet shape is determined by a balance of hydrostatic and curvature pressures. Such a balance is well understood to underlie the leading-order droplet geometry, and much of the following argument has appeared, for instance, in the work of Tanner (1979) and Voinov (1999).

We write r for the radial coordinate and $h(r)$ for the height of the droplet's surface. To leading order in $h/\ell_c \lesssim 1$, the pressure immediately inside the droplet satisfies $p(r) = -\sigma\nabla^2 h$. Balancing hydrostatic and curvature pressures of the surface requires that

$$\sigma\,\partial_z\nabla^2 h = \sigma\,\frac{\partial_r\nabla^2 h}{\partial_r h} = \rho g. \tag{2.6}$$

https://doi.org/10.1017/jfm.2026.11664 Published online by Cambridge University Press

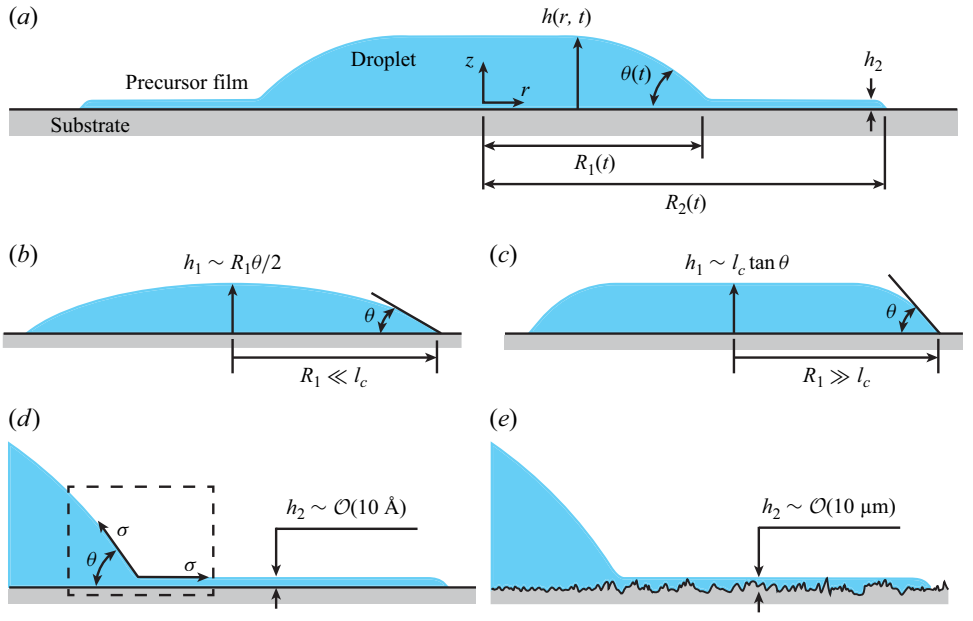


Figure 1. Schematic of the physical system under investigation. (*a*) The droplet forms the rounded shape (2.7) of radius R_1, contact angle θ and maximum depth $h_1 = h(0) \ll \ell_c$. In the case of total wetting, the droplet is generally preceded by a precursor film of thickness $h_2 \ll h_1$ and radius $R_2 \geqslant R_1$. (*b*) A small droplet ($R_1 \ll \ell_c$) approximately forms a spherical cap with a maximum depth $h_1 \sim R_1\theta/2$. (*c*) A large droplet ($R_1 \gg \ell_c$) is shaped more like a flat disk, with a depth $h_1 \sim \ell_c \tan\theta$ that is approximately constant for $r < R_1 - \ell_c$. (*d*) If the substrate is smooth, a microscopic precursor film arises with thickness h_2 on the molecular scale. (*e*) If the substrate is rough, a Darcy precursor film arises with thickness comparable to the roughness height (in the case of our experiments, approximately 10 μm). The zoom box in (*d*) illustrates the net horizontal surface tension force $f = \sigma(1 - \cos\theta) \sim \sigma\theta^2/2$ acting radially outward on the apparent contact line; such a force is present on both smooth and rough substrates. In all cases, the radius R_1 grows with time, while θ and h_1 decrease.

By non-dimensionalising and enforcing axisymmetry, one may find the solution

$$h(r) = \frac{I_0(R_1) - I_0(r)}{I_1(R_1)} \tan\theta, \tag{2.7}$$

which has an associated total droplet volume

$$V = \int_0^{R_1} 2\pi r h(r)\,\mathrm{d}r = \left(\pi R_1^2 \frac{I_0(R_1)}{I_1(R_1)} - 2\pi R_1\right)\tan\theta. \tag{2.8}$$

Here, $R_1 = R_1/\ell_c$ is the dimensionless horizontal droplet radius, θ is the apparent contact angle at the droplet–film interface and I_0 and I_1 are modified Bessel functions. As one might expect, this height profile always describes a rounded shape with radial extent R_1. Its qualitative behaviour is best understood by investigating the small- and large-droplet limits. The Bessel functions I_0 and I_1 have the following asymptotic behaviour for small and large arguments:

$$\begin{aligned} x \ll 1 \quad &\Longrightarrow \quad I_0(x) \sim 1 + x^2/4, \quad I_1(x) \sim x/2, \\ x \gg 1 \quad &\Longrightarrow \quad I_0(x) \sim I_1(x) \sim e^x/\sqrt{2\pi x}. \end{aligned} \tag{2.9}$$

As evident from these asymptotic expressions, the qualitative shape of the droplet greatly depends on the relative magnitudes of R_1 and ℓ_c. When $R_1 \ll \ell_c$ and $\theta \lesssim \pi/4$, the profile (2.7) asymptotes to that of a spherical cap with radius of curvature $R_{cap} \sim R_1/\theta$

https://doi.org/10.1017/jfm.2026.11664 Published online by Cambridge University Press

and maximum height $h_1 \sim R_1\theta/2$, as illustrated in figure 1(*b*). When $R_1 \gg \ell_c$, the profile asymptotes to that of a flat puddle of height $h_1 \sim \ell_c \tan\theta$, except in the boundary region $|R_1 - r| \lesssim \ell_c$, where it decays to zero (figure 1*c*).

The profile (2.7) interpolates smoothly between these two limits. In particular, if the radius of an initially small droplet grows to exceed ℓ_c, the droplet transitions through a sequence of increasingly flattened spherical shapes until reaching the pancake-like form depicted in figure 1(*c*) (Cazabat & Cohen Stuart 1986; Ehrhard 1993). The precise cross-over radius is of the order of ℓ_c, but has been reported to depend weakly on the droplet volume (Cazabat & Cohen Stuart 1986).

2.2. *Existing models for total wetting by small droplets*

The modern understanding of small droplet spreading ($R_1 \ll \ell_c$) over a flat substrate began with the experimental work of Hoffman (1975), who observed the scaling $\dot{R} \sim \theta^3$. An initial attempt to rationalise Hoffman's findings was provided by Voinov (1976) and Tanner (1979), based on a lubrication approximation of the droplet dynamics. Their work rationalised Tanner's laws (sometimes known as the Hoffman–Voinov–Tanner laws) for the spreading of a small droplet on a rough substrate: $R \sim V^{3/10}t^{1/10}$ and $\theta \sim V^{1/10}t^{-3/10}$. A more complete description of the droplet motion – and the first to correctly account for the precursor film – was subsequently provided by Hervet & de Gennes (1984). They argue that small droplets maintain the shape of a spherical cap (see figure 1(*b*)) as they are slowly stretched outward by contact line forces. In turn, the rate of spreading can be deduced from the droplet's internal energy balance.

The argument of Hervet & de Gennes proceeds as follows. Suppose the droplet boundary advances at a speed U. On one hand, there is a force $f = \sigma(1 - \cos\theta) \approx \sigma\theta^2/2 > 0$ per unit arclength along the apparent contact line – arising from unbalanced surface tension forces when the droplet meets the surface at an angle $\theta \lesssim \pi/4$ (see figure 1(*d*)) – which does work $w \sim \sigma\theta^2 U/2$ per unit arclength. Hervet & de Gennes argue that this work is dissipated primarily along the outer edge of the droplet. To model this process, they define a radial coordinate $\chi = R_1 - r$ measuring the distance (inward) from the edge. In order to ensure that the droplet surface (at $z = \theta\chi$) travels with velocity U, a linear shear profile $u(\chi, z) \sim Uz/\theta\chi$ is adopted. The resulting energy dissipation rate is not integrable, so the authors fix upper and lower cutoff lengths in χ, say, L and a, respectively. Physically, one expects $L \lesssim \ell_c$ and for a to be on the molecular scale; indeed, one generally needs a microscopic cutoff length in order to regularise dissipation near a moving contact line (Huh & Scriven 1971). The energy dissipation per unit arclength is thus

$$\int_a^L \int_0^{\theta\chi} \mu \left(\frac{\partial u}{\partial z}\right)^2 \mathrm{d}z\,\mathrm{d}\chi = \int_{\ell_0}^L \frac{\mu U^2}{\theta\chi}\,\mathrm{d}\chi = \frac{\mu}{\theta}\log(L/a)U^2. \tag{2.10}$$

Writing $\ell_D = \log(L/a)$, they thus deduce the evolution equation $\dot{R}_1 \sim U \sim \theta^3/2\ell_D$, consistent with the predictions of Hoffman (1975), Voinov (1976) and Tanner (1979).

Hervet & de Gennes went a step further and estimated the cutoff lengths L and a based on the micro-structure of the droplet-film transition on a smooth substrate. They thus find a logarithmic correction to Hoffman's scaling, of the form

$$\theta^3 \sim \dot{R}_1 \log\left([\dot{R}_1]^{2/3}\right). \tag{2.11}$$

The work of Eggers & Stone (2004) has since offered a slight correction to the scaling coefficients predicted by Hervet & de Gennes, and separate work by Hocking & Rivers (1982), Hocking (1983), Cox (1986*a*, *b*), Snoeijer (2006), Chan *et al.* (2013) and Luo & Gao (2025) has clarified the local structure of a moving contact line. The physical

https://doi.org/10.1017/jfm.2026.11664 Published online by Cambridge University Press

model furnished by the spreading laws of Hervet & de Gennes and subsequent work on the contact line problem remains well supported by a variety of experimental investigations of liquid spreading on smooth substrates (Ngan & Dussan V. 1982; Chen 1988; Chen & Wada 1989; Dussan V., Ramé & Garoff 1991; Marsh, Garoff & Dussan V. 1993; Ramé & Garoff 1996).

The work of Cazabat & Cohen Stuart (1986) showed that the same spreading laws apply to the spreading of small droplets on rough substrates, where the Darcy precursor film plays a role similar to the precursor film on a smooth substrate. Their findings are consistent with the more general theoretical treatment of Starov *et al.* (2002*a*, *b*, 2003) of small droplet spreading on rough substrates, and subsequent experimental investigations of the same (Grzelakowski *et al.* 2009; Gambaryan-Roisman 2014; Dorbolo 2021). Notably, spreading on deep, porous substrates ($h_2 \gtrsim h, \ell_c$) does not yield the same universal behaviour (Davis & Hocking 1998; Starov *et al.* 2002*c*, 2003; Frank & Perré 2012; Chebbi 2021). In the same vein, we note that the logarithmic correction (2.11) to Hoffman's scaling depends on the microstructure of the droplet-film transition on a smooth surface. To our knowledge, evidence for such a logarithmic correction has yet to be observed for spreading on rough substrates.

2.3. *Existing models for total wetting by large droplets*

For large-droplet spreading ($R \gg \ell_c$), the most widely accepted model is that of Lopez *et al.* (1976), who apply a lubrication approximation to model the interior of the droplet, away from the apparent contact line. The height profile h thus satisfies

$$\partial_t h(r) = -\frac{1}{3\mu}\boldsymbol{\nabla}\cdot\left(h^3\boldsymbol{\nabla}(\sigma\boldsymbol{\nabla}^2 h - \rho g h)\right). \tag{2.12}$$

Lopez *et al.* proceed by supposing that surface tension is negligible in the relatively flat droplet interior (see figure 1(*c*)). The resulting physics is then exactly that of a viscous gravity current, as discussed in § 1, giving rise to the scaling $R_1 \sim V^{3/8}t^{1/8}$.

Subsequent work has adapted this gravity-driven model in various ways. Ehrhard & Davis (1991) suggested that gravitational overpressure is resisted by edge-localised energy dissipation, rather than the bulk dissipation of Lopez *et al.* (1976), and so recovered a scaling $R_1 \sim t^{1/7}$. Subsequent authors have argued that bulk dissipation should be dominant, and thus that the widely observed $R_1 \sim t^{1/8}$ scaling should emerge (Hocking 1992, 1994; Bonn *et al.* 2009). In a different direction, Voinov (1995, 1999) suggested perturbatively correcting this gravity-driven model to better account for the effect of surface tension near the edge of the droplet. Voinov posits two distinct regimes in the droplet: a gravity-driven interior, like that of Lopez *et al.*, and a quasi-static meniscus region. The two regimes are connected by asymptotically matching height profiles at their interface, and Voinov uses the contact angle predicted by the fully quasi-equilibrium droplet profile (2.7) as a boundary condition for the outer region.

It has been observed by Cazabat & Cohen Stuart (1986) that, if a droplet's radius R_1 grows to exceed the capillary length during the course of spreading, it transitions rapidly from the small-droplet scaling $R_1 \sim t^{1/10}$ to the large-droplet scaling $R_1 \sim t^{1/8}$. Ehrhard (1993) observed similar behaviour, but argued that their data support the $R_1 \sim t^{1/7}$ large-droplet scaling derived by Ehrhard & Davis (1991). In either case, according to the current understanding of these two regimes, such a transition would entail a rapid change from a quasi-equilibrium, edge-driven flow to a dynamic, overpressure-driven flow. We revisit this problem in § 5, where we see that the model presented here rationalises the results of Cazabat & Cohen Stuart (1986) with an edge-driven spreading mechanism valid for both small and large drops.

https://doi.org/10.1017/jfm.2026.11664 Published online by Cambridge University Press

2.4. *Existing models for partial wetting on smooth substrates*

While the total wetting regime remains our primary focus, it is worth outlining the close connection between the spreading of totally wetting droplets (with spreading parameter $S > 0$) and the relaxation to equilibrium of partially wetting droplets (with $S < 0$). Droplets in both regimes exhibit a leading-order geometry of the form described in § 2.1, as well as unbalanced contact line forces that drive the droplet spreading. These similarities suggest that the present model can be adapted to describe the relaxation to equilibrium of partially wetting droplets, a case we return to in § 5.

Partially wetting droplets do not generally give rise to precursor films (Bonn *et al.* 2009), so are marked by a well-defined contact line where the liquid, substrate, and ambient vapour all meet. Such droplets tend toward a static equilibrium as they spread, in which the drop meets the substrate at a contact angle $\theta_{eq} > 0$ prescribed by Young's law (2.3). Various models have been proposed to rationalise the spreading of partially wetting drops as they relax into equilibrium (de Gennes, Hua & Levinson 1990; Brochard-Wyart & Gennes 1992; Petrov & Petrov 1992; de Ruijter *et al.* 1997, 1999; Eggers 2005). The most recent and comprehensive work on the subject is that of Durian *et al.* (2022), which extends the model of de Ruijter *et al.* (1999) to account for droplets of arbitrary horizontal radius.

Consistent with prior literature, Durian *et al.* posit that spreading is driven by either capillary or gravitational forces, depending on the horizontal radius of the drop. As in our own model, however, they posit that spreading is resisted by a combination of bulk and edge-localised energy dissipation, and thereby recover smooth transitions between previously observed scaling laws. For small droplets, they find an equation of the form

$$\left(\alpha R_1^9/V^3 + \kappa R_1^6/V^2\right)\dot{R}_1 = 1 - (R_1/R_{1,eq})^6 \tag{2.13}$$

for system-dependent parameters α, $\kappa > 0$. For large droplets, they similarly find

$$\left(\alpha R_1^7/V^3 + \kappa R_1^4/V^2\right)\dot{R}_1 = 1 - (R_1/R_{1,eq})^4. \tag{2.14}$$

A key point in the derivation of Durian *et al.* is that the form of the edge-localised energy dissipation in the droplet is not the same as that prescribed by Hervet & de Gennes (1984) for totally wetting droplets. Following de Ruijter *et al.* (1999), the edge-localised energy dissipation for a partially wetting droplet is posited to take the form

$$D_{edge} \sim \kappa R_1(\dot{R}_1)^2, \tag{2.15}$$

independent of the contact angle θ. By comparison, recall that Hervet & de Gennes suggest the form $D_{edge} \sim \beta R_1(\dot{R}_1)^2/\theta$ for totally wetting droplets. We note that the form (2.15) is consistent with resistance generated by corrugation of the contact line.

We revisit the question of partial wetting in § 5, where we show that, by adapting our model to account for substrate-dependent contact line forces, one can interpolate between the small-droplet prediction (2.13) and the large-droplet prediction (2.14) using a single edge-driven mechanism.

2.5. *Washburn's law for precursor films on rough substrates*

Precursor films on rough substrates – which we refer to as Darcy precursor films – can be understood as viscous flows through a shallow, porous medium (Gambaryan-Roisman 2014). Such flows are governed by Darcy's law (Darcy 1856; Whitaker 1986):

$$\overline{u} = -\frac{k}{\mu\phi}\left(\nabla p - f\right). \tag{2.16}$$

https://doi.org/10.1017/jfm.2026.11664 Published online by Cambridge University Press

Here, $\overline{u}$ is the local mean velocity of the fluid, k is the permeability of the medium, ϕ is the porosity (i.e. void fraction) of the medium and f is the volumetric force within the precursor film.

Volume conservation requires that $\overline{u} \propto 1/r$, and matching $\overline{u}|_{R_2} = \dot{R}_2$ yields $\overline{u} = R_2\dot{R}_2/r$. The volumetric force f is prescribed by the surface tension acting on the inner and outer boundaries of the precursor film. To calculate it, we model the film as a ring of independent, radial strands of fluid, each subtending an angle $\mathrm{d}\theta$. The total tension applied to such a strand is $SR_2\,\mathrm{d}\theta$, where S is the roughness-dependent spreading parameter of our fluid over the given substrate. The tension-per-unit-radius is thus $SR_2(R_2 - R_1)^{-1}\,\mathrm{d}\theta$. If we suppose that the tension is uniformly distributed across the cross section of fluid at radius r, then the volumetric force is

$$f = \frac{SR_2(R_2 - R_1)^{-1}\,\mathrm{d}\theta}{h_2 r\,\mathrm{d}\theta} = \frac{\sigma s R_2/r}{R_2 - R_1}, \tag{2.17}$$

where we define $s = S/h_2\sigma$ for convenience. Finally, if one neglects the pressure gradient in (2.16), one finds the following variant of Washburn's law (Washburn 1921):

$$\dot{R}_2 = \frac{ks}{\phi}\,\frac{1}{R_2 - R_1}, \qquad \Delta R = R_2 - R_1 \sim \sqrt{kst/\phi}, \tag{2.18}$$

after making the approximation $\dot{R}_2 \gg \dot{R}_1$ and adopting our non-dimensionalisation. In practice, while the particular scaling $\Delta R \sim t^{1/2}$ can be achieved with certain combinations of liquids and substrates, previous authors have observed a range of exponents between 0.25 and 0.5 (Cazabat & Cohen Stuart 1986; Dorbolo 2021). We will build upon this model through consideration of gravitational overpressure from the droplet bulk, which will play a critical role in rationalising our experimental results. In § 5, we revisit the problem in order to demonstrate how the $R_2 \sim t^{3/10}$ spreading reported by Dorbolo (2021) can be rationalised with the same model.

3. Experiments: large droplets on rough substrates

We investigate the spreading of a liquid droplet and its associated Darcy precursor film over a rough surface. We focus here on the total wetting of roughened glass surfaces by large droplets ($R_1 \gg \ell_c$) of silicone oil. As we discuss in § 4, this case allows us to most clearly distinguish our proposed spreading model from the existing gravity-driven paradigm for large droplets (Lopez *et al.* 1976). We will apply our model to rationalise existing datasets for small droplets, smooth substrates and partial wetting in § 5.

3.1. *Methodology*

Rough surfaces were made by hand-lapping 75×75 mm^2 square sections of borosilicate glass on a slurry of course-grain silicone-carbide lapping compound and water. Two types of lapping compound with different grain sizes were used to make surfaces of different roughness: the first surface (S60) was sanded with 60 grit (or 250 μm) compound, and the second surface (S100) was sanded with 100 grit (120 μm). The resulting surfaces were visibly 'frosted' (or opaque). The surfaces are characterised by their permeability k and porosity (i.e. void fraction) ϕ. It is shown that S60 and S100 have $k/\phi = 3.28 \times 10^{-5}$ cm^2 and $k/\phi = 2.03 \times 10^{-5}$ cm^2, respectively, implying the pore size decreases as the grit of the lapping compound increases (or the average size of the lapping aggregate decreases). A laser-scanning confocal microscope (VK-X250, Keyence) was used to visualise the topography of the roughened glass substrates. A sample two-dimensional projection of

https://doi.org/10.1017/jfm.2026.11664 Published online by Cambridge University Press

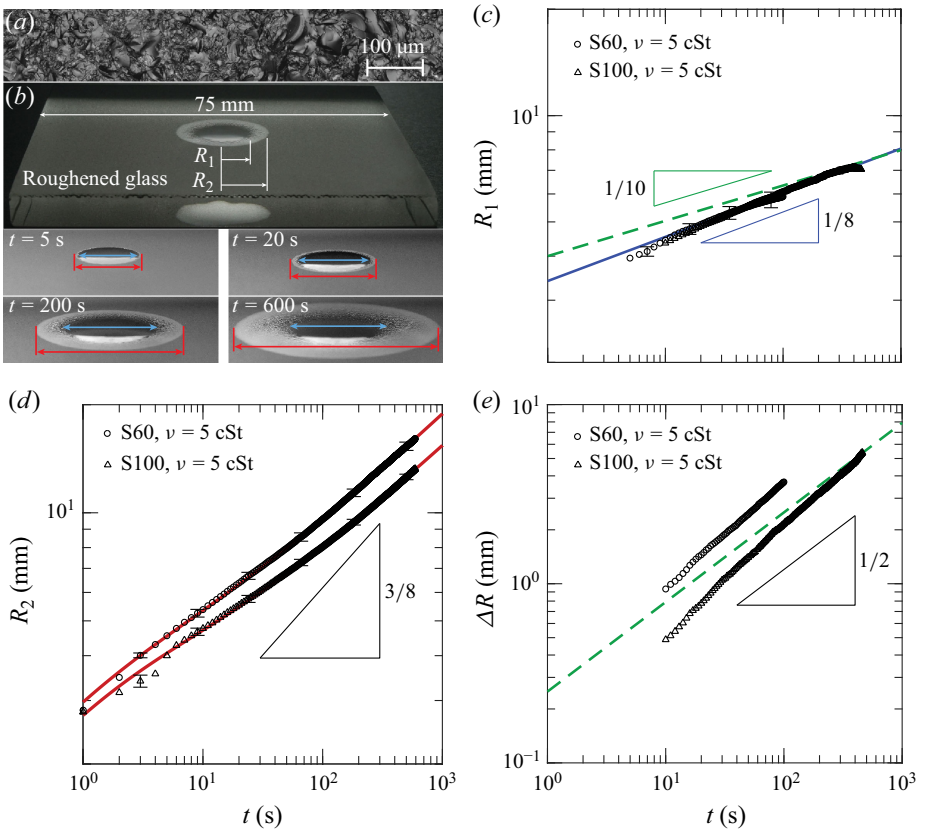


Figure 2. (*a*) Confocal microscope scan of the surface S60, a borosilicate glass square sanded with 60 grit silicone-carbide lapping compound. (*b*) Annotated image of a silicone oil droplet wetting the surface S100, sanded instead with 100 grit compound. Shown below are several snapshots of the spreading process, with the drop diameter $2R_1$ (blue arrows) and precursor film diameter $2R_2$ (red arrows) indicated. (*c–e*) Time evolution of the drop radius R_1, the film radius R_2, and their difference $\Delta R = R_2 - R_1$, for a 5 μl silicone oil droplet ($\nu = 5$ cSt, $\sigma = 20$ mN m^{-1}, $\rho = 0.913$ g cm^{-3}) wetting both S60 and S100. The solid blue line in (*c*) represents the roughness-independent scaling $R_1 \sim t^{1/8}$ predicted for large droplets ($R_1 \gg \ell_c$), and the dashed green line represents the scaling $R_1 \sim t^{1/10}$ predicted for small droplets ($R_1 \ll \ell_c$). These observations are consistent with our experiments being in the large-droplet regime. The solid red lines in (*d*) are fits of R_2 measurements, equal to $R_2(t) = At^{3/8}/[\log(Bt + C)]^{1/2}$ for surface-dependent parameters A, B, C. For the surface S100, the fitting coefficients are $A = 2.99$ mm s$^{-3/8}$, $B = 0.63$ s^{-1} and $C = 2.62$. For the surface S60, the fitting coefficients are $A = 3.80$ mm s$^{-3/8}$, $B = 1.33$ s^{-1} and $C = 3.79$. We rationalise the values of these parameters in Appendix A. We observe that neither curve adheres to the $t^{3/8}$ power law recovered from neglecting log factors in this fit. Finally, the dashed line in (*d*) represents the scaling $\Delta R(t) \sim t^{1/2}$ predicted by Washburn's law of wicking, which is inconsistent with our observations. We note that previous experiments of viscous droplet spreading also report strong deviations from Washburn's law (Cazabat & Cohen Stuart 1986; Dorbolo 2021). We rationalise these deviations in § 5.

a microscope scan for S60 is shown in figure 2(*a*). Surface asperities exhibit a hierarchy of length scales from tens of nanometres to hundreds of micrometres. The areal footprint of the large-scale asperities observed in figure 2(*a*) for S60 are comparable to the derived pore size $k/\phi = 3.28 \times 10^{-5}$ cm^2. The root-mean-squared (r.m.s.) roughness height for the S60 surface measured using the confocal microscope was 7.6 μm and the average lateral length scale (an auto-correlation length) was 56.7 μm. Due to limitations in equipment availability, we were unable to make the same measurement for S100. Since the lapping

https://doi.org/10.1017/jfm.2026.11664 Published online by Cambridge University Press

process was the same, however, we can scale by the ratio of (square root) permeabilities, $0.79 \approx 45\ \mu\text{m}/57\ \mu\text{m}$, to estimate that the r.m.s. roughness height is 6.0 μm and the lateral length scale is 44.9 μm for S100.

3.2. *Experimental results*

In our primary experiments, a $V = 5$ μl drop of silicone oil (63148-62-9, Millipore Sigma), with $\sigma = 20\ \text{mN m}^{-1}$, $\rho = 0.913\ \text{g cm}^{-3}$, $\mu = 4.6$ mPa s (or $\nu = \mu/\rho = 5.0$ cSt) and initial radius $R_1(t = 0) \approx 3.0$ mm, was gently placed on the roughened glass substrate. Here, the capillary length ℓ_c is 1.5 mm and the capillary velocity is $u_c = \sigma/\mu = 4.3\ \text{m s}^{-1}$. We note that the silicone oils we use are non-volatile at normal (ambient) temperature and pressure, with 'no detectable vapour pressure' (European Centre for Ecotoxicology and Toxicology of Chemicals (ECETOC) 2011), and they totally wet borosilicate glass (Dorbolo 2021). A secondary series of experiments with liquids of higher viscosity is reported in § 3.3, and supports the conclusions drawn from our primary experiments.

The shape of the drop as it wet the substrate was monitored using a 4 Mpixel digital camera (Lumix GH5, Panasonic) at an image acquisition rate of 1 Hz, with a diffuse spot light for backlit illumination. The camera was positioned at an acute angle above the horizontal plane to promote detection of the droplet bulk from reflection. A sample image of the droplet on S60 is shown in figure 2(*b*) with the droplet radius R_1 and precursor film radius R_2 labelled. An edge detection algorithm developed in MATLAB (MathWorks) was used to extract the droplet bulk radius R_1 and precursor film radius R_2 from each image. Namely, the image background is first subtracted to enhance contrast with the spreading liquid. Images are then binarised using the method of Otsu (1979), which adequately discriminates the bright precursor film from the relatively dark background, yielding an estimate of R_2. A similar procedure is used to extract the droplet radius R_1, after inverting the image to isolate the darker droplet bulk. Measurements of the droplet diameter $2R_1$ and precursor film diameter $2R_2$ are annotated in blue and red, respectively, on the sample snapshots in figure 2(*b*).

At least five experimental trials, each consisting of 600 images taken over 600 s, were performed for both roughened glass surfaces. The average values of $R_1(t)$ and $R_2(t)$ across the repeat trials are shown in figures 2(*c*) and 2(*d*). Error bars represent the standard deviation in the measurements of $R_1(t)$ and $R_2(t)$ across the repeated trials. These repeatability errors are no larger than ±5 % for all times t. Sample images of the spreading droplet on S60 at different times t are shown above figures 2(*c*) and 2(*d*). This imaging setup is ideal for capturing droplet spreading on our opaque, roughened surfaces, where there is clear contrast between the droplet, film and substrate, as illustrated in figure 2. However, it is less effective for visualising droplet spreading on smooth, transparent glass substrates, where contrast is significantly reduced. Measurements of R_2 for spreading on a smooth substrate require techniques with much larger spatial resolution, given that $h_2 \sim \mathcal{O}(10\ \text{Å})$ in this case. We do not pursue such measurements here, as there are several previous investigations of droplet spreading on smooth substrates using methods such as ellipsometry or X-ray reflectivity that can accurately resolve both radii (Bascom, Cottingdon & Singleterry 1964; Daillant *et al.* 1988; Cazabat *et al.* 1997; Popescu *et al.* 2012). In § 5, we will revisit existing datasets of Cazabat & Cohen Stuart (1986) and de Ruijter *et al.* (1999) for droplet spreading over smooth substrates.

Figure 2(*c*) demonstrates the evolution of R_1 with time, and figure 2(*d*) shows the evolution of R_2. Measurements for the surfaces of different roughness are represented with different symbols (black triangles for S100, black circles for S60). For all observed times t, the droplet radius R_1 is large ($R_1 \gg \ell_c = 1.5$ mm). Consistent with previous studies (Lopez *et al.* 1976; Cazabat & Cohen Stuart 1986; Voinov 1999), fits of $R_1(t)$ in this

https://doi.org/10.1017/jfm.2026.11664 Published online by Cambridge University Press

ν (cSt)	ρ (kg m^{-3})	μ (cP)	σ (mN m^{-1})	ℓ_c (mm)	u_c (m s^{-1})
5	913	4.6	20	1.49	4.38
10	930	9.3	20	1.48	2.15
50	960	48.0	20	1.46	0.42

Table 1. Material properties of the different test fluids in § 3.3.

large-droplet regime demonstrate a power-law trend with an exponent of 1/8, independent of the surface roughness. This fit is shown with a solid blue curve in figure 2(*c*). A dashed green curve with a power-law exponent of 1/10, the predicted scaling for small droplets (Voinov 1976; Tanner 1979; Hervet & de Gennes 1984), is shown for comparison.

For all values of t and k, R_2 exhibits excellent agreement with a function of the form $R_2(t) = At^{3/8}/[\log(Bt + C)]^{1/2}$. These fits are shown with red solid curves in figure 2(*d*) for both surfaces. For the surface S100, the parameters $A = 2.99$ mm s$^{-3/8}$, $B = 0.63$ s^{-1} and $C = 2.62$ produce good overlap with the measurements; the relative r.m.s. deviation between the measurements and the fit is 0.68 %. For the surface S60, the fitting coefficients $A = 3.80$ mm s$^{-3/8}$, $B = 1.33$ s^{-1} and $C = 3.79$ yield a r.m.s. deviation of 0.39 %. We note that the numerical value of C is negligible beyond $t \gtrsim 10$ s; we rationalise the observed scalings of R_1 and R_2 in § 4 and the observed values of A and B in Appendix A. For the sake of comparison, we show in figure 2(*e*) that neither set of experiments satisfies the $\Delta R = R_2 - R_1 \sim t^{1/2}$ scaling predicted by the classic version of Washburn's law (see § 2.5).

A few features of figures 2(*c*) and 2(*d*) merit further comment. First, we note that the droplet and film radii can only be clearly distinguished beyond $t \sim 5$–10 s, indicating that the Darcy precursor film is not fully developed until that time. Similarly, the droplet depth becomes comparable to the roughness scale when $t \gtrsim 400$ s for S100 and when $t \gtrsim 100$ s for S60. We believe these limitations account for the slight deviations of both $R_1(t)$ and $R_2(t)$ from predictions for $t \lesssim 5$ s and those of $R_1(t)$ for $t \gtrsim 400$ s. Next, the evolution of R_2 depends on the substrate roughness k; as the substrate roughness decreases from S60 to S100, R_2 also decreases for all t. Physically, this trend reflects the fact that resistance to flow decreases with greater substrate permeability. Finally, figure 2(*d*) highlights the need for the $(\log t)^{1/2}$ term in the denominator of the scaling for $R_2(t)$; the spreading is not well described by a $t^{3/8}$ scaling.

3.3. *Dynamic similarity*

We here present the results of a secondary series of experiments, in which we compare the spreading rates of silicone oils of different viscosities on the same rough substrate S100. We perform experiments using $\nu = 10$ and $\nu = 50$ cSt silicone oil, to complement our data for $\nu = 5$ cSt silicone oil. The material properties of all three fluids are listed in table 1. The same experimental setup is used, but with longer acquisition times. For the $\nu = 10$ cSt silicone oil, 600 images are collected at an acquisition rate of 0.5 frames per second, equivalent to 20 min of data collection. For the $\nu = 50$ cSt silicone oil, 600 images are collected at an acquisition rate of 0.1 frames per second, equivalent to 100 minutes of data collection.

Figures 3(*a*) and 3(*b*) illustrate the evolution of the droplet radius $R_1(t)$ and the Darcy precursor film radius $R_2(t)$, respectively, for silicone oils of viscosity $\nu = 5$, 10 and 50 cSt on the roughened surface S100. When the radii $R_1(t)$ and $R_2(t)$ are normalised with respect to the capillary length ℓ_c and plotted with respect to a dimensionless time $\hat{t} = t\ell_c/u_c$, the measurements overlap closely, indicating that the spreading dynamics

https://doi.org/10.1017/jfm.2026.11664 Published online by Cambridge University Press

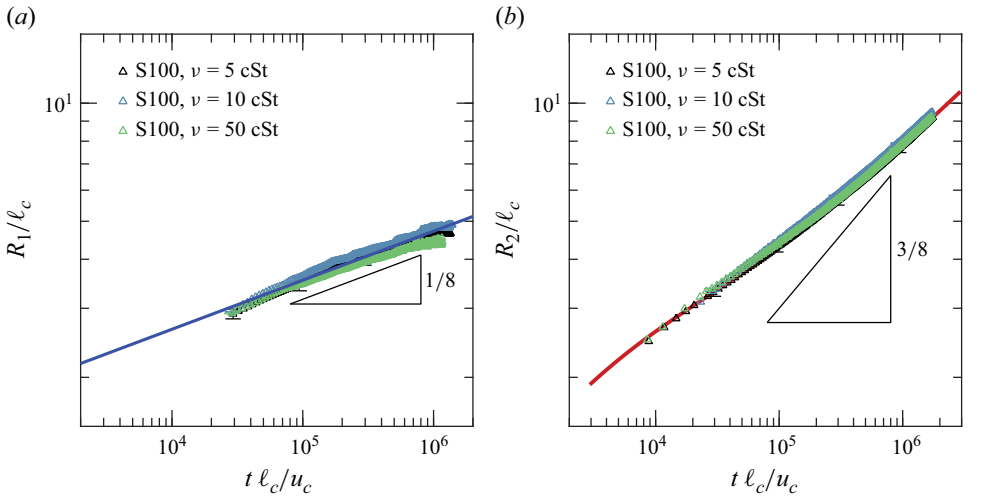


Figure 3. Evolution of (*a*) the droplet radius $R_1(t)$ and (*b*) the Darcy precursor film radius $R_2(t)$ for silicone oils of kinematic viscosity $\nu = 5$, 10 and 50 cSt on the surface S100. When non-dimensionalised with respect to the capillary length ℓ_c and plotted against the dimensionless time $\hat{t} = t\ell_c/u_c$, all three measurements of R_1 align closely with a single $R_1(\hat{t})/\ell_c \sim \hat{t}^{1/8}$ curve (blue), and all three measurements of R_2 align closely with a single $R_2(\hat{t}) = A\hat{t}^{3/8}/[\log(B\hat{t} + C)]^{1/2}$ curve (red), where $A = 0.10$, $B = 2.0 \times 10^{-4}$ and $C = 2.50$.

is dynamically similar. As before, the droplet radius exhibits a $R_1(\hat{t})/\ell_c \sim \hat{t}^{1/8}$ scaling, and the Darcy precursor film fits follows the trend $R_2(\hat{t})/\ell_c = A\hat{t}^{3/8}/[\log(B\hat{t} + C)]^{1/2}$. Fits of the data yield dimensionless fitting coefficients of $A = 0.10$, $B = 2.0 \times 10^{-4}$ and $C = 2.50$. Because all three experiments are dynamically similar to the $\nu = 5$ cSt case, the discussion in Appendix A can be used to rationalise these coefficients.

4. Theoretical model

We proceed by developing a theoretical model of viscous droplet spreading that both rationalises our own experimental observations and provides insight into prior experimental studies. The core feature of our model is that the droplet maintains a quasi-equilibrium state as it evolves, with curvature and hydrostatic pressure in balance according to the calculated profile (2.7). A similar assumption was applied in the small-droplet limit by Tanner (1979), Hervet & de Gennes (1984) and others; in this limit, the droplet maintains the shape of a spherical cap, thereby minimising surface area. We remark that the height profile we deduce from this balance is not novel (Tanner 1979; Voinov 1999); the novelty of our approach is the use of (2.7) as an evolving quasi-equilibrium, driven by unbalanced interfacial forces acting along the droplet's edge. We discuss in turn the dynamics of the spreading droplet and the Darcy precursor film that precedes it when it spreads on a rough substrate.

4.1. *Dynamics of the droplet edge*

We first derive an expression for the speed at which the droplet's edge advances, using a simple scaling argument. The present section simplifies and generalises the argument of Hervet & de Gennes (1984) presented in § 2.2.

We suppose here that viscous dissipation is not necessarily confined to the vicinity of the droplet edge, as posited by Hervet & de Gennes (1984), but that some component of the dissipation may occur throughout the droplet bulk. The total dissipation may thus be

https://doi.org/10.1017/jfm.2026.11664 Published online by Cambridge University Press

expressed as

$$D = D_{edge} + D_{bulk}. \tag{4.1}$$

Lifting the assumption of edge-localised dissipation is natural in the Stokes-flow limit, where one expects instantaneous equilibration of the flow field throughout the droplet bulk; indeed, splitting the total energy dissipation into 'edge' and 'bulk' contributions was previously suggested by de Ruijter *et al.* (1999) and Durian *et al.* (2022) for the case of partial wetting, and bulk dissipation was assumed in the gravity-driven model of Lopez *et al.* (1976). For a simple, concrete flow field that exhibits the properties we seek, one could imagine that, away from the edges, a large droplet would evolve as a slow Poiseuille-type current of the form

$$u(r, z) \sim U \frac{r}{R_1} \frac{z}{h_1} \left(2 - \frac{z}{h_1}\right). \tag{4.2}$$

We emphasise that we do not prescribe such a flow profile. The model we present relies only on scaling arguments, and thus rationalises the observed spreading rates of viscous droplets without detailed knowledge of the droplets' flow profiles.

Suppose Φ is the average local rate of energy dissipation throughout the droplet bulk, and $U \sim \dot{R}_1$ is the rate of spreading. Then the bulk dissipation rate is given by

$$D_{bulk} \sim \alpha V \Phi \sim \alpha \mu h_1 R_1^2 \frac{U^2}{h_1^2} \sim \frac{\alpha \mu R_1^2 I_1(R_1) U^2}{(I_0(R_1) - 1) \tan\theta}, \tag{4.3}$$

for some constant $\alpha > 0$. The above formula is deduced by substituting $V \sim h_1 R_1^2$ and $h_1 = h|_{r=0}$, noting that $V \sim h_1 R_1^2$ holds for both small and large droplets. We remark that a similar result would follow if we instead used the full expression (2.8) to estimate the volume in (4.3); in particular, the asymptotic limits of our model would remain unchanged.

An expression for D_{edge} can be derived using the analytical argument of Hervet & de Gennes (1984), presented in § 2.2. For the sake of completeness, however, we illustrate how the form of D_{edge} can be deduced from a similar scaling argument as that of D_{bulk}. If dissipation occurs within a distance L of the edge, then it occurs over the solid of rotation carved out by a triangle of height $H = L \tan\theta$ and area $A = 1/2 L^2 \tan\theta$; this solid has a volume $V_{edge} \sim R_1 H L$, and we expect the total dissipation within it to take the form

$$D_{edge} \sim \beta V_{edge} \Phi_{edge} \sim \beta \mu R_1 H L \frac{U^2}{H^2} = \beta \mu R_1 \frac{U^2}{\tan\theta}, \tag{4.4}$$

for some constant $\beta > 0$. Setting $\beta = \log(L/a)$ recovers the result of Hervet and de Gennes (see § 2.2). We remark that, *a priori*, there might also be a contribution of the form (2.15) proposed by de Ruijter *et al.* (1999) and Durian *et al.* (2022), dependent only on the spreading speed U and the arclength $2\pi R_1$ of the apparent contact line and independent of the apparent contact angle θ. Such a contribution might correspond to micro-physics at the droplet–film interface, at length scales $\ell \ll L$; for the analogous case of partially wetting drops on rough substrates, for instance, one expects resistance to arise from microscopic corrugation of the contact line (de Gennes *et al.* 2003). In all, the edge-localised dissipation would take the more general form

$$D_{edge} \sim \beta \mu R_1 \frac{U^2}{\tan\theta} + \kappa \mu R_1 U^2, \tag{4.5}$$

for some constant $\kappa > 0$. In any case, the total energy dissipation D takes the form

https://doi.org/10.1017/jfm.2026.11664 Published online by Cambridge University Press

$$D = D_{bulk} + D_{edge} \sim \left(\alpha \frac{R_1^2 I_1(R_1)}{(I_0(R_1) - 1)\tan\theta} + \beta \frac{R_1}{\tan\theta} + \kappa R_1 \right) \mu U^2. \tag{4.6}$$

One can simplify this expression in our limits of interest. First, we assume that $\beta R_1/\tan\theta \gg \kappa R_1$, because $\theta \ll 1$. This assumption can otherwise be justified by considering that, in the small-droplet limit, the β term must be dominant in order to recover the widely corroborated scaling predictions of Hoffman (1975), Voinov (1976) and Tanner (1979). Secondly, the remaining contribution of D_{edge} does not change the asymptotic form of D in either the large- or small-droplet limit. In the limit $R_1 \gg \ell_c$, the α term is quadratic in R_1 and thus dominates the edge dissipation. In the limit $R_1 \ll \ell_c$, both the α and the β terms are linear in R_1, and one can simply augment $\alpha \mapsto \alpha + \beta$ to account for both. Since we are ultimately interested in these asymptotic limits, we proceed as though edge dissipation is accounted for in the value of $\alpha > 0$ for small droplets.

The work done in moving the contact line is $W \sim \sigma(1 - \cos\theta) R_1 U$. The droplet's internal energy balance is given by $D \sim W$, which upon rearrangement yields

$$\frac{R_1 I_1(R_1)}{I_0(R_1) - 1} \dot{R}_1 = 2\alpha^{-1}(\tan\theta - \sin\theta) \sim \alpha^{-1}\theta^3, \tag{4.7}$$

for $\theta \lesssim \pi/4$ and the same constant $\alpha > 0$ as above. We employ the asymptotic formulas (2.9) to deduce the small- and large-drop limits of this result. For small droplets ($R_1 \ll \ell_c$), we have $R_1 I_1(R_1)/[I_0(R_1) - 1] \to 2 = \text{const.}$, so (4.7) recovers the $\dot{R}_1 \sim \theta^3$ scaling of Hoffman (1975). For large droplets, $R_1 I_1(R_1)/[I_0(R_1) - 1] \to R_1$, so (4.7) yields the modified scaling $\dot{R}_1 \sim \theta^3/R_1$.

Using the expression (2.8) for the droplet volume to eliminate θ, we find

$$\dot{R}_1 = \alpha^{-1} \frac{I_0(R_1) - 1}{R_1 I_1(R_1)} \left(\frac{V/\pi}{R_1^2 \frac{I_0(R_1)}{I_1(R_1)} - 2R_1} \right)^3. \tag{4.8}$$

We note that the liquid volume that drains into the precursor film (over either smooth or rough substrates) is negligible over the time scales of interest. Indeed, because the roughness (or microscopic) scale h_2 is small relative to the droplet depth h_1, the liquid volume contained within the film is negligible with respect to that within the droplet,

$$V_{film} = h_2 R_2^2 \ll h_1 R_1^2 \sim V, \tag{4.9}$$

noting that the scaling $V \sim h_1 R_1^2$ holds for both small and large droplets. Provided (4.9) holds, the change in droplet volume V is negligible, so (4.8) yields an expression for the evolution of the droplet radius. We note that the system could alternatively be closed by an equation of the form $\dot{V} = -\dot{V}_{film} = -2\pi\phi h_1(R_1\dot{R}_1 - R_2\dot{R}_2)$, where ϕ is the porosity of the rough substrate (and $\phi = 1$ for smooth substrates). We do not pursue this direction further at present, and instead take V to be constant.

The physical picture we propose can be summarised as follows, for both large and small drops. At all times, hydrostatic and curvature pressure gradients are in balance throughout the droplet, except in the immediate vicinity of the apparent contact line. At the apparent contact line, interfacial forces act to stretch the droplet uniformly outward. The work done by these interfacial forces is dissipated inside the droplet, and the associated energy balance determines the rate of spreading.

The basic physical picture is common to both small and large droplets; different scalings arise in the two limits only because the relationship between V, θ and R_1 changes according to (2.8). In the small-droplet limit $R_1 \ll \ell_c$, the asymptotic formulas (2.9) show

https://doi.org/10.1017/jfm.2026.11664 Published online by Cambridge University Press

Small droplet, 2-D ($R_1 \ll \ell_c$)	Large droplet, 2-D ($R_1 \gg \ell_c$)	Small droplet, 1-D ($R_1 \ll \ell_c$)	Large droplet, 1-D ($R_1 \gg \ell_c$)
$\dot{R}_1 \sim \theta^3$	$\dot{R}_1 \sim R_1^{-1}\theta^3$	$\dot{R}_1 \sim \theta^3$	$\dot{R}_1 \sim R_1^{-1}\theta^3$
$R_1 \sim V^{3/10}t^{1/10}$	$R_1 \sim V^{3/8}t^{1/8}$	$R_1 \sim V^{3/7}t^{1/7}$	$R_1 \sim V^{3/5}t^{1/5}$
$\theta \sim V^{1/10}t^{-3/10}$	$\theta \sim V^{1/4}t^{-1/4}$	$\theta \sim V^{1/7}t^{-2/7}$	$\theta \sim V^{2/5}t^{-1/5}$
$h_1 \sim V^{2/5}t^{-1/5}$	$h_1 \sim V^{1/4}t^{-1/4}$	$h_1 \sim V^{4/7}t^{-1/7}$	$h_1 \sim V^{2/5}t^{-1/5}$
Wicking-driven Darcy precursor films			
$\Delta R \sim k^{1/2}s^{1/2}t^{1/2}$	$\Delta R \sim k^{1/2}s^{1/2}t^{1/2}$	$\Delta R \sim k^{1/2}s^{1/2}t^{1/2}$	$\Delta R \sim k^{1/2}s^{1/2}t^{1/2}$
Overpressure-driven Darcy precursor films			
$R_2 \sim \frac{k^{1/2}V^{-1/10}t^{3/10}}{\sqrt{\log kV^{-1/5}t^{3/5}}}$	$R_2 \sim \frac{k^{1/2}V^{1/8}t^{3/8}}{\sqrt{\log kV^{1/4}t^{3/4}}}$	$\Delta R \sim k^{1/2}V^{-1/7}t^{2/7}$	$\Delta R \sim k^{1/2}V^{1/5}t^{2/5}$

Table 2. Scalings predicted by our model in various limits of interest, for both one-dimensional and axisymmetric two-dimensional systems. Here, R_1, h_1 and θ are the horizontal radius, depth and apparent contact angle of the droplet bulk, R_2 is the radius of the Darcy precursor film on a rough substrate and $\Delta R = R_2 - R_1$. The scalings reported for $\dot{R}_1$, R_1, h_1 and θ are predicted to hold for droplets totally wetting either smooth or rough substrates, but we clarify that we do not predict the spreading rate of a microscopic precursor film on a smooth substrate. The $\dot{R}_1 \sim \theta^3$ scaling of Hoffman (1975) and Hervet & de Gennes (1984) arises in the small-droplet limit in both one- and two-dimensional systems. The $R_1 \sim V^{3/10}t^{1/10}$ and $\theta \sim V^{1/10}t^{-3/10}$ laws of Voinov (1976) and Tanner (1979) arise in the small-droplet limit in two dimensions. The $R_1 \sim V^{3/7}t^{1/7}$ scaling of Tanner (1979) and McHale *et al.* (1995) arises in the small-droplet limit in one dimension. The $\Delta R \sim t^{1/2}$ law of Washburn (1921) arises in the limit of a tension-driven film dynamics. The $R_1 \sim V^{3/8}t^{1/8}$ scaling observed by Lopez *et al.* (1976) arises for large droplets in two dimensions.

that the right-hand side of (4.8) scales as V^3/R_1^9, so the evolution equation reduces to the $R_1(t) \sim V^{3/10}t^{1/10}$ scaling of Hoffman (1975), Voinov (1976) and Tanner (1979). For large droplets, the right-hand side of (4.8) scales as V^3/R_1^7, which yields a scaling $R_1(t) \sim V^{3/8}t^{1/8}$ familiar from viscous gravity currents. We summarise the small- and large-droplet limits of our model in table 2, in both one- and two-dimensional geometries. Since the derivation presented here depends on scaling arguments, one should expect (4.8) to hold in both limits, but not necessarily to yield exact predictions for the small-to-large-droplet transition. We return to the latter question in § 5.

We note that our predicted $R_1 \sim V^{3/8}t^{1/8}$ scaling for large droplets carries the same prefactor as that of gravity currents. Indeed, reintroducing units to our scaling yields

$$R_1 \sim \ell_c\left(V/\ell_c^3\right)^{3/8}(tu_c/\ell_c)^{1/8} = \ell_c^{-1/4}u_c^{1/8}V^{3/8}t^{1/8} = (\rho g/\mu)^{1/8}V^{3/8}t^{1/8}. \tag{4.10}$$

Notably, despite the dynamics of our model being driven by interfacial forces, σ necessarily drops out from the final scaling. We can rationalise this phenomenon as follows. Recall that the horizontal contact line force per unit arclength is $f \sim \sigma\theta^2$. If one fixes the droplet radius R_1 and depth h_1, then the equilibrium droplet profile (2.7) shows that the contact angle decreases with increasing surface tension, as $\theta \sim h_1/\ell_c \sim h_1(\rho g/\sigma)^{1/2}$. Thus, the total interfacial force scales as

$$f \sim \sigma\theta^2 \sim \sigma(h_1/\ell_c)^2 \sim \rho g h_1^2, \tag{4.11}$$

independent of σ. As a consequence, when $R_1 \gg \ell_c$, one cannot distinguish our edge-driven 'capillary current' model from traditional gravity currents on the basis of $R_1(t)$ alone. Specifically, capillary currents (for which $Bo \lesssim 1$) that are wide with respect to the

https://doi.org/10.1017/jfm.2026.11664 Published online by Cambridge University Press

capillary length obey precisely the same surface-tension-independent spreading law (1.1) satisfied by viscous gravity currents (for which $Bo \gg 1$). We distinguish between the two models in the following subsection, by testing their respective predictions for the evolution of a Darcy precursor film when a droplet spreads on a rough substrate.

4.2. *Dynamics of a Darcy precursor film on a rough substrate*

We model the Darcy precursor film as a viscous, two-dimensional flow through a homogeneous, porous medium, subject to Darcy's law (2.16). Here, we modify the statement of Washburn's law (2.18) to account for the pressure gradient across the precursor film, associated with overpressure in the droplet bulk. Similar calculations were carried out by Clarke *et al.* (2002) and Starov *et al.* (2002*a*, 2003) for small droplets on deep and shallow porous substrates, respectively, but we here give a more detailed account of the time-evolving overpressure within the droplet.

Following the same argument as § 2.5, we know that the local mean velocity $\overline{u}$ and volumetric force f within the precursor film must satisfy $\overline{u},\ f \propto 1/r$. These are two of the three terms appearing in Darcy's law (2.16), so we deduce that the third term must have the same dependence, i.e. $\nabla p \propto 1/r$. Matching the pressure conditions at the leading and trailing edge of the film, $p|_{r=R_2} = 0$ and $p|_{r=R_1} = -\sigma \nabla^2 h(R_1)$, we find

$$p = -\sigma\big(\nabla^2 h\big)(R_1)\,\frac{\log(r/R_2)}{\log(R_1/R_2)} = \frac{\sigma V/\pi}{R_1^2 - 2R_1\frac{I_1(R_1)}{I_0(R_1)}}\,\frac{\log(r/R_2)}{\log(R_1/R_2)}. \tag{4.12}$$

Inserting this expression into (2.16) and using the expression (2.17) for f, we deduce a modified evolution equation for the radius of the precursor film

$$R_2\dot{R}_2 = \frac{k}{\phi}\left(\frac{V/\pi}{(R_1^2 - 2R_1\frac{I_1(R_1)}{I_0(R_1)})\log(R_2/R_1)} + \frac{sR_2}{R_2 - R_1}\right). \tag{4.13}$$

We note that our theory is based on the assumption of a precursor film, in which case $\Delta R = R_2 - R_1 > 0$.

Depending on surface chemistry, the system obeys one of two different dynamics. First, in the limit where surface tension dominates (roughly, if $\sigma s \gg \rho g \ell_c$), we recover the classic variant of Washburn's law, derived in § 2.5. In the limit where hydrostatic pressure dominates ($\sigma s \ll \rho g \ell_c$), we approximate $\log(R_2/R_1) \sim \log R_2$ in order to write

$$\log(R_2)R_2\dot{R}_2 \sim \frac{k}{\phi}\frac{V}{R_1^2 - 2R_1\frac{I_1(R_1)}{I_0(R_1)}}. \tag{4.14}$$

In the large-droplet limit $R_1 \gg \ell_c$, for instance, we find $\log(R_2)R_2^2 \sim (k/\phi)\alpha^{1/4}V^{1/4}t^{3/4}$. In general, if $y^n \log y = x$, then $y = \exp(n^{-1}W(nx))$, where W is the Lambert W-function (Corless *et al.* 1996). Since $W(x) \sim \log x - \log\log x$ for large arguments, we find

$$R_2(t) \sim \frac{(k/\phi)^{1/2}\alpha^{1/8}V^{1/8}t^{3/8}}{\sqrt{\log[(k/\phi)\alpha^{1/4}V^{1/4}t^{3/4}]}} \sim \frac{t^{3/8}}{\sqrt{\log t}}. \tag{4.15}$$

Our experimental results in § 3 are consistent with this scaling, and would appear to disqualify simpler power-law scalings. The small-droplet limit follows similarly, giving $R_2 \sim t^{3/10}/(\log t)^{1/2}$. All scalings are reported in table 2.

We note that the logarithmic correction to our predicted R_2 scaling is necessary to rationalise our experimental results in § 3. This correction arises from the circular geometry of the system, as it does in the scalings found for coalescence of circular droplets

https://doi.org/10.1017/jfm.2026.11664 Published online by Cambridge University Press

in the work of Eggers, Lister & Stone (1999). Indeed, the one-dimensional equivalent of our system – corresponding to the 'fluid stripe' experiments of McHale *et al.* (1995) – gives a modified power law with no logarithmic factors.

Finally, we remark that the $R_2 \sim t^{3/8}/(\log t)^{1/2}$ scaling regime is not consistent with the gravity-driven hypothesis introduced by Lopez *et al.* (1976) and currently understood to underlie the $R_1 \sim V^{3/8}t^{1/8}$ scaling of large droplets (Bonn *et al.* 2009; Popescu *et al.* 2012). Gravity-driven spreading implies a horizontal pressure gradient across the droplet radius, and thus a relatively low pressure $p|_{r=R_1} \ll \rho g h_1$ at the edge. By contrast, the $R_2 \sim t^{3/8}/(\log t)^{1/2}$ scaling regime arises owing to hydrostatic overpressure $p|_{r=R_1} \approx \rho g h_1$ at the droplet edge, consistent with our quasi-equilibrium model. In demonstrating the existence of an $R_2 \sim t^{3/8}/(\log t)^{1/2}$ film spreading regime, our experiments in § 3 would thus appear to distinguish the large-droplet limit of our edge-driven model from gravity currents.

5. Broader applications: small droplets, smooth substrates and partial wetting

We proceed by presenting three datasets from the literature, for which the present work may offer a valuable new perspective. In turn, these datasets characterise the spreading of a Darcy precursor film ahead of a small droplet on a rough substrate (Dorbolo 2021), the early-time spreading of partially wetting droplets on smooth substrates (de Ruijter *et al.* 1999; Durian *et al.* 2022) and the transition from small- to large-droplet regimes on smooth substrates (Cazabat & Cohen Stuart 1986). All droplets under consideration are shallow ($h \lesssim \ell_c$), and the descriptors 'small' and 'large' indicate how their horizontal radii compare with the capillary length.

In figure 4(*a*), we reproduce a downsampled version of the data recorded by Dorbolo (2021) for the spreading of a Darcy precursor film ahead of a small drop of silicone oil ($\nu = \mu/\rho = 20$ cSt) on a frosted glass substrate. The glass is sold commercially as 'SATINOVO® MATT' (Saint-Gobain Glass 2024), and Dorbolo reported it as having a r.m.s. height variation of 2.34 μm and a characteristic distance between peaks of 34 ± 10 μm, somewhat finer than either of the substrates used in our experiments. The precursor film undergoes three characteristic spreading regimes over 120 days ($\sim 10^7$ s) of observation. First, it undergoes an intermediate time regime ($t \lesssim 10^5$ s) with a clear distinction between droplet bulk and Darcy precursor film, the latter advancing according to $R_2 \sim t^{3/10}$. Dorbolo inferred that this spreading was driven by wicking, with a deviation from Washburn's law (§ 2.5) caused by irregular roughness elements. After the droplet bulk sinks into the surface roughness (10^5 s $\lesssim t \lesssim 10^7$ s), the film spreads according to $R_2 \sim t^{3/20}$, a scaling previously observed by Cazabat & Cohen Stuart (1986). Finally, for $t \gtrsim 10^7$ s, the film appears to stops spreading. While the latter two regimes are beyond the scope of our work, the initial spreading regime is consistent with our model.

The initial radius $R_1(t = 0)$ of the droplet is not reported, but extrapolating the scaling $R_2 \sim t^{3/10}$ backwards indicates that $R_1(t = 0) < R_2(t = 1\text{ s}) \lesssim 1.5\ell_c$, so it can be assumed that the droplet is relatively small. The prediction $R_2 \sim t^{3/10}$ is thus consistent with our own prediction $R_2 \sim t^{3/10}/(\log t)^{1/2}$ in the long-time limit for Darcy precursor films driven by small droplets. We note that, while the logarithmic factor was necessary to explain short-time behaviours (particularly $t \lesssim 10^2$ s) in our own experiment, the logarithm grows very slowly for large arguments. One thus expects it to become negligible over the much longer time scale at which the initial spreading regime is observed in Dorbolo's experiment ($\sim 10^5$ s). More generally, we note that the prior experiments of Cazabat & Cohen Stuart (1986) observed a range of exponents for this process between 0.25

https://doi.org/10.1017/jfm.2026.11664 Published online by Cambridge University Press

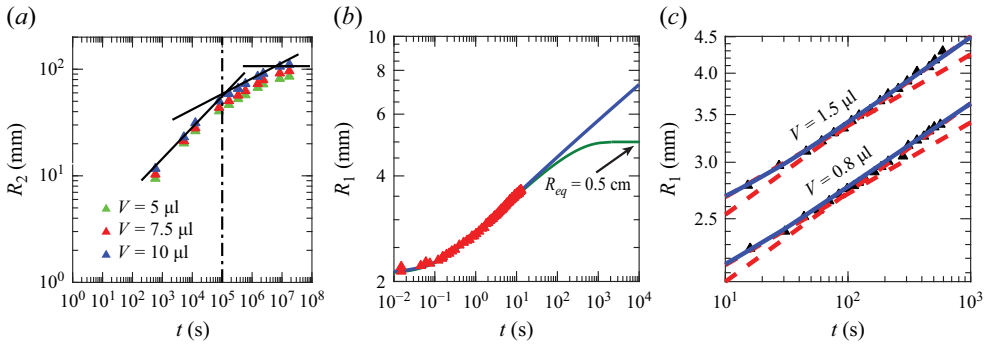


Figure 4. (*a*) Downsampled version of the data recorded by Dorbolo (2021) for the spreading of a Darcy precursor film ahead of a small drop of 20 cSt silicone oil on a frosted glass substrate. The radius R_2 of the film undergoes three distinct spreading regimes: $R_2 \sim t^{3/10}$ for the intermediate time regime ($t \lesssim 10^5$ s) of present interest, $R_2 \sim t^{3/20}$ after the droplet bulk sinks into the surface roughness (10^5 s $\lesssim t \lesssim 10^7$ s); and $R_2 \sim$ const. at very late times ($t \gtrsim 10^7$ s). Although Dorbolo originally inferred that the first spreading regime was driven by wicking, with deviations from Washburn's law (§ 2.5) caused by irregular roughness elements, we note that the observed scaling $R_2 \sim t^{3/10}$ is consistent with our predictions for overpressure-driven Darcy precursor films ahead of small drops. (*b*) The data recorded by de Ruijter *et al.* (1999) for the spreading of a partially wetting, viscous drop of DBP on a smooth PET substrate, along with two fitted curves reproduced from Durian *et al.* (2022): the predicted behaviour of the droplet if the equilibrium radius were $R_{eq} = 0.5$ cm (green); and the predicted early-time spreading behaviour, independent of R_{eq} (blue). A natural extension of our work to partially wetting drops yields the evolution equation (5.1), which reproduces the predictions of Durian *et al.* (2022) for both large and small drops with a purely edge-driven model. (*c*) Data reported by Cazabat & Cohen Stuart (1986) for the spreading of viscous drops of methyl-terminated poly dimethylsiloxane (PMS) on smooth glass, depicting the small-to-large-droplet transition as R_1 exceeds the capillary length. Also shown are the asymptotic $R_1 \sim t^{1/10}$ and $R_1 \sim t^{1/8}$ curves (dashed red) for both $V = 1.5$ and $V = 0.8$ µl, reproduced from Cazabat & Cohen Stuart (1986), and the predictions of our own model for both cases (blue). Specifically, we report the predictions of the evolution equation (4.8) augmented with the three dissipation terms present in (4.6), with the fitted coefficients $\alpha = 1$, $\beta = 15$, $\kappa = 150$.

and 0.5. Our model suggests that these exponents might arise from a combination of overpressure-driven and wicking-driven spreading.

We turn now to droplet spreading on smooth substrates. Figure 4(*b*) depicts the data recorded by de Ruijter *et al.* (1999) for the spreading of partially wetting droplets. Specifically, they studied the spreading of a small droplet of dibutyl phthalate (DBP; $\mu =$ 19.6 mP s, $\sigma = 34.3$ mN m^{-1}) on a smooth polyethylene terephthalate (PET) substrate. Under normal conditions, DBP partially wets PET with a very low equilibrium contact angle, and does not give rise to a precursor film. This dataset was revisited in the recent work of Durian *et al.* (2022), in order to validate their model for the relaxation of partially wetting droplets into equilibrium. In figure 4(*b*), we reproduce fitted curves calculated by Durian *et al.* (2022). The green curve corresponds to an example choice of equilibrium drop radius $R_{eq} = 0.5$ cm, and the blue curve corresponds to the asymptotic early-time behaviour (which is independent of R_{eq}) predicted by their model.

If we were to retain the modified edge dissipation term (2.15) in our own model and focus on the early stage of droplet spreading ($R_{eq} \gg R_1$), then we would find an equation of the form

$$\left(\alpha \frac{R_1^3 I_0(R_1) - 2R_1^2 I_1(R_1)}{V^3(I_0(R_1) - 1)} + \frac{\kappa}{V^2}\right)\left(R_1^2 \frac{I_0(R_1)}{I_1(R_1)} - 2R_1\right)^2 \dot{R}_1 = \text{const.}, \tag{5.1}$$

https://doi.org/10.1017/jfm.2026.11664 Published online by Cambridge University Press

with the constant determined by the wetting properties of the system. It can be verified that this equation recovers the limits (2.14) and (2.13) in the large- and small-droplet limits, respectively. We note that a slightly more involved analysis (incorporating certain elements of Durian *et al*. (2022) would yield an evolution equation appropriate for characterising the full (early and late stage) dynamics.

Despite these limitations, examination of the data of Cazabat & Cohen Stuart (1986) indicates that our model yields a close match to observations of the small-to-large transition for droplets totally wetting smooth substrates. Figure 4(*c*) depicts the data recorded by Cazabat & Cohen Stuart for the spreading of small droplets of methyl-terminated poly dimethylsiloxane (PMS; $\nu = 20\,\mathrm{cSt}$, $\sigma = 22\,\mathrm{mN\,m^{-1}}$) on smooth, hydrophilic surfaces (microscope glass slides). As each droplet crosses the threshold between small and large horizontal radius (at a value $R_1 \sim \ell_c$ that is weakly volume-dependent), Cazabat & Cohen Stuart report a transition from $R_1 \sim t^{1/10}$ to $R_1 \sim t^{1/8}$. We show two of their experiments for which the transition is most visible, corresponding to drop volumes $V = 0.78\,\mu\mathrm{l}$ and $V = 1.5\,\mu\mathrm{l}$. For each, we show asymptotic $R_1 \sim t^{1/10}$ and $R_1 \sim t^{1/8}$ scalings that approximately fit the early- and late-time data (dashed red curves). We also show our own predictions based on numerical integration of (4.8), augmented with all three dissipation terms present in (4.6), and the fitted values of $\alpha = 1$, $\beta = 15$, $\kappa = 150$. One can confirm that $\beta/\tan\theta \gtrsim \kappa$ for all time, as required for the small-droplet limit to exhibit $R_1 \sim t^{1/10}$ growth (see § 4.1).

6. Discussion

The present work suggests a new physical picture for the spreading of viscous droplets over flat substrates, either rough or smooth. In the small-droplet limit, our model converges to that of Hervet & de Gennes (1984). It thereby recovers the scalings $\dot{R}_{drop} \sim \theta^3$ and $R_{drop} \sim V^{3/10} t^{1/10}$ of Hoffman (1975), Voinov (1976) and Tanner (1979) for small droplets totally wetting flat substrates, with V the droplet volume and θ its evolving contact angle. In the large-droplet limit, our model provides a self-consistent, edge-driven alternative to the predominant gravity-driven paradigm (Lopez *et al.* 1976; Bonn *et al.* 2009; Popescu *et al.* 2012). The resulting capillary currents can be distinguished from traditional gravity currents through the droplet's pressure profile, which directly influences the spreading of the Darcy precursor film on a rough substrate. The observed scaling of the precursor film radius would thus seem to support the inference of edge-driven capillary currents.

There are various natural extensions to the present model. For one, much of the analysis for a one-dimensional droplet-film system follows similarly to the two-dimensional case. If we write x for the horizontal spatial coordinate and assume the droplet to be symmetric across $x = 0$, we find expressions for the droplet height profile and volume,

$$h(x) = \frac{\cosh(R_1) - \cosh(x)}{\sinh(R_1)}\,\tan\theta, \qquad V = 2(R_1\coth(R_1) - 1)\tan\theta, \tag{6.1}$$

the following analogues to (4.7) and (4.8):

$$R_1\coth(R_1/2)\dot{R}_1 = \alpha\theta_d^3, \qquad R_1\coth(R_1/2)\dot{R}_1 = \alpha\left(\frac{V/2}{R_1\coth R_1 - 1}\right)^3, \tag{6.2}$$

and the following evolution equation for the precursor film:

$$\dot{R}_2 = \frac{k}{2\phi}\,\frac{V(R_1 - \tanh R_1)^{-1} + 2s}{R_2 - R_1}, \tag{6.3}$$

https://doi.org/10.1017/jfm.2026.11664 Published online by Cambridge University Press

all written in the dimensionless units (2.4). The right-hand side of table 2 reports scalings for this system. Notably, we recover the $R_1 \sim V^{3/7}t^{1/7}$ scaling for thin fluid stripes reported in the experiments of McHale *et al.* (1995) and first predicted by Tanner (1979).

Our discussion in § 5 also suggests how the present work might inform the modelling of partially wetting droplets, and shows that our predictions for partially wetting droplets are consistent with those of Durian *et al.* (2022). We have restricted attention here to the early spreading regime ($R_1 \ll R_{eq}$), and have reported data only for a liquid–substrate pair with very small equilibrium contact angle ($\theta_{eq} \ll 1$). Further experiments could test the predictions of our edge-driven model for liquid–substrate pairs with larger equilibrium contact angle, or for the relaxation of a partially wetting drop into equilibrium. Finally, a few of the scalings predicted in table 2 have yet to be observed: the $R_1 \sim V^{3/5}t^{1/5}$ scaling predicted for thick fluid stripes and the $\Delta R \sim V^{-1/7}t^{2/7}$ and $\Delta R \sim V^{1/5}t^{2/5}$ scalings predicted for pressure-driven precursor films in one dimension. These predictions could conceivably be tested with droplet spreading experiments similar to our own.

Acknowledgements. D.D. acknowledges the support of an NDSEG Graduate Fellowship. L.W. acknowledges the support of the Natural Sciences and Engineering Research Council of Canada (NSERC) (PDF-587339-2024). *Cette recherche a été financée par le Conseil de recherches en sciences naturelles et en génie du Canada (CRSNG) (PDF-587339-2024).*

Declaration of interests. The authors report no conflict of interest.

Appendix A. Eliminating free parameters in our model fit

We can rationalise the fitting parameters inferred from the experiments of § 3 by appropriately matching coefficients against our predictions from § 4. The observed scalings of R_1 in § 3 yield the coefficient $\alpha \approx 3.45$ in the relation (4.7), independent of surface roughness. Now, comparing the fitted curve $R_2(t) \sim At^{3/8}/[\log(Bt + C)]^{1/2}$ from § 3 against the predicted expression (4.15) for $R_2(t)$, after tracking constants through the analysis of § 4.2 and reintroducing units, shows that

$$A = (16/3)^{1/2}\,(\pi/2)^{3/8}(k/\phi)^{1/2}\alpha^{1/8}V^{1/8}\ell_c^{-3/4}u_c^{3/8}. \tag{A1}$$

Plugging in the values $\alpha = 3.45$ and $V = 5$ µl yields $k/\phi \approx 2.03 \times 10^{-5}$ cm^2 for the surface S100 and $k/\phi \approx 3.28 \times 10^{-5}$ cm^2 for S60. These estimates are consistent with known values of the permeability for similar materials (e.g. sand, fine gravel) (Bear 1988), and they satisfy the predicted ratio of grit numbers

$$\frac{k_{S100}}{k_{S60}} = \frac{2.03 \times 10^{-5}\ \text{cm}^2}{3.28 \times 10^{-5}\ \text{cm}^2} = 0.6 \pm 2\ \% = \frac{60}{100} \pm 2\ \%. \tag{A2}$$

Moreover, the porosity value $k/\phi \approx 3.28 \times 10^{-5}$ cm^2 inferred for S60 aligns closely with its measured auto-correlation length $L_{S60} = 56.7$ µm, specifically $\sqrt{k_{S60}} = 57.2\,\mu\text{m} = L_{S60} \pm 1$ %. Furthermore, assuming the ratio $k_{S100}/k_{S60} = 60/100$ and inferring the value of A for each surface, we observe that the predicted value for the ratio A_{S100}/A_{S60} holds within 2 %. Assuming $k_{S60} = L_{S60}^2$ and inferring the value of A for S60 yields the measured value within 1 %.

In turn, we can rationalise our measured value of B in the fit $R_2(t) \sim At^{3/8}/[\log(Bt + C)]^{1/2}$. We neglect the time shift C, as its effect largely disappears for $t \gtrsim 10$ s. To estimate B, we revise the approximation made in (4.14). Writing $\overline{R}_1 = R_1(t = 0) \approx 3.0$ mm, we now estimate $\log(R_2/R_1) \sim \log(R_2/\overline{R}_1)$ to recover

https://doi.org/10.1017/jfm.2026.11664 Published online by Cambridge University Press

$$R_2 \sim \frac{\beta t^{3/8}}{\sqrt{\log[\beta^2 t^{3/4}/(\overline{R}_1)^2]}} = \frac{\sqrt{4/3}\,\beta t^{3/8}}{\sqrt{\log[\beta^{8/3}(\overline{R}_1)^{-8/3} t]}} \tag{A3}$$

for some as-of-yet unknown $\beta > 0$. Setting $A = (4/3)^{1/2}\beta$, we thus predict the value of B to be $B_{est.} = (3/4)^{4/3}(A/\overline{R}_1)^{8/3}$. For S100, this yields $B_{est.} = 1.28\ \mathrm{s}^{-1}$, which compares favourably with the best-fit value $B = 1.33\ \mathrm{s}^{-1}$. For S60, this yields $B_{est.} = 0.67\ \mathrm{s}^{-1}$, again comparable to the best-fit value $B = 0.63\ \mathrm{s}^{-1}$.

References

Bascom, W., Cottingdon, R. & Singleterry, C. 1964 Dynamic surface phenomena in the spontaneous spreading of oils on solids. In *Contact Angle, Wettability, and Adhesion* (ed. F.M. Fowkes), pp. 355–379. American Chemical Society.

Bear, J. 1988 *Dynamics of Fluids in Porous Media*, Dover Civil and Mechanical Engineering Series, vol. 61. Dover.

Biance, A., Clanet, C. & Quéré, D. 2004 First steps in the spreading of a liquid droplet. *Phys. Rev. E* **69**, 016301.

Bonn, D., Eggers, J., Indekeu, J., Meunier, J. & Rolley, E. 2009 Wetting and spreading. *Rev. Mod. Phys.* **81** (2), 739–805.

Brochard-Wyart, F. & de Gennes, P.G. 1992 Dynamics of partial wetting. *Adv. Colloid Interface* **39**, 1–11.

Cazabat, A. & Cohen Stuart, M. 1986 Dynamics of wetting: effects of surface roughness. *J. Phys. Chem-US* **90** (22), 5845–5845.

Cazabat, A., Gerdes, S., Valignat, M. & Villette, S. 1997 Dynamics of wetting: from theory to experiment. *Interface Sci.* **5**, 129–139.

Chan, T.S., Srivastava, S., Marchand, A., Andreotti, B., Biferale, L., Toschi, F. & Snoeijer, J.H. 2013 Hydrodynamics of air entrainment by moving contact lines. *Phys. Fluids* **25** (7), 074105.

Chebbi, R. 2021 *Absorption and Spreading of a Liquid Droplet Over a Thick Porous Substrate*. ACS Omega XXXX.

Chen, J. 1988 Experiments on a spreading drop and its contact angle on a solid. *J. Colloid Interface Sci.* **122** (1), 60–72.

Chen, J. & Wada, N. 1989 Wetting dynamics of the edge of a spreading drop. *Phys. Rev. Lett.* **62** (26), 3050–3053.

Clarke, A., Blake, T.D., Carruthers, K. & Woodward, A. 2002 Spreading and imbibition of liquid droplets on porous surfaces. *Langmuir* **18** (8), 2980–2984.

Corless, R.M., Gonnet, G.H., Hare, D.E.G., Jeffrey, D.J. & Knuth, D.E. 1996 On the Lambert W function. *Adv. Comput. Math.* **5** (1), 329–359.

Cox, R.G. 1986a The dynamics of the spreading of liquids on a solid surface. Part 1. Viscous flow. *J. Fluid Mech.* **168**, 169–194.

Cox, R.G. 1986b The dynamics of the spreading of liquids on a solid surface. Part 2. Surfactants. *J. Fluid Mech.* **168**, 195–220.

Daillant, J., Benattar, J.J., Bosio, L. & Leger, L. 1988 Final stages of spreading of polymer droplets on smooth solid surfaces. *Europhys. Lett.* **6** (5), 431.

Darcy, H. 1856 *Les Fontaines Publiques de lA ville de Dijon*. V. Dalmont.

Davis, S.H. & Hocking, L.M. 1998 Spreading and imbibition of viscous liquid on a porous base. *Phys. Fluids* **11** (1), 1994.

Dorbolo, S. 2021 The wetting properties of frosted glass. *Pap. Phys.* **13**, 130006.

Durian, S.C.L., Dillavou, S., Markin, K., Portales, A., Maldonado, B.O.T., Irvine, W.T.M., Arratia, P.E. & Durian, D.J. 2022 Spatters and spills: spreading dynamics for partially wetting droplets. *Phys. Fluids* **34** (1), 012112.

Dussan V., E.B., Ramé, E. & Garoff, S. 1991 On identifying the appropriate boundary conditions at a moving contact line: an experimental investigation. *J. Fluid Mech.* **230**, 97–116.

Eddi, A., Winkels, K.G. & Snoeijer, J.H. 2013 Short time dynamics of viscous drop spreading. *Phys. Fluids* **25** (1), 013102.

Eggers, J. 2005 Contact line motion for partially wetting fluids. *Phys. Rev. E* **72** (6), 061605.

Eggers, J., Lister, J.R. & Stone, H.A. 1999 Coalescence of liquid drops. *J. Fluid Mech.* **401**, 293–310.

Eggers, J. & Stone, H.A. 2004 Characteristic lengths at moving contact lines for a perfectly wetting fluid: the influence of speed on the dynamic contact angle. *J. Fluid Mech.* **505**, 309–321.

https://doi.org/10.1017/jfm.2026.11664 Published online by Cambridge University Press

EHRHARD, P. 1993 Experiments on isothermal and non-isothermal spreading. *J. Fluid Mech.* **257**, 463–483.
EHRHARD, P. & DAVIS, S.H. 1991 Non-isothermal spreading of liquid drops on horizontal plates. *J. Fluid Mech.* **229**, 365–388.
European Centre for Ecotoxicology and Toxicology of Chemicals (ECETOC) 2011 Linear polydimethylsiloxanes: CAS no. 63148-62-9 (Second Edition). Available at: https://www.ecetoc.org/wp-content/uploads/2014/08/JACC-055-Linear-Polydimethylsiloxanes-CAS-No.-63148-62-9-Second-Edition.pdf. JACC Report No. 55.
FRANK, X. & PERRÉ, P. 2012 Droplet spreading on a porous surface: a lattice Boltzmann study. *Phys. Fluids* **24** (4), 042101.
GAMBARYAN-ROISMAN, T. 2014 Liquids on porous layers: wetting, imbibition and transport processes. *Curr. Opin. Colloid Interface Sci.* **19** (4), 320–335.
DE GENNES, P.G. 1985 Wetting: statics and dynamics. *Rev. Mod. Phys.* **57**, 827–863.
DE GENNES, P.G., BROCHARD-WYART, F. & QUERE, D. 2003 *Capillarity and Wetting Phenomena: Drops, Bubbles, Pearls, Waves*. Springer.
DE GENNES, P.G., HUA, X. & LEVINSON, P. 1990 Dynamics of wetting: local contact angles. *J. Fluid Mech.* **212**, 55–63.
GLASS, S.-G. 2024 *SATINOVO® MATT: Matt-Finished Translucent Glass*. Product Brochure.
GRZELAKOWSKI, C., BEN JAZIA, D., LEBEAU, B., VONNA, L., DUPUIS, D. & HAIDARA, H. 2009 On the influence of pore structure on the free-imbibition of sessile drops into nanoporous substrates. *Langmuir* **25** (10), 5855–5860.
HARDY, W.B. 1919 III. The spreading of fluids on glass. *Lond. Edinb. Dublin Phil. Mag. J. Sci.* **38** (223), 49–55.
HERVET, H. & DE GENNES, P.G. 1984 The dynamics of wetting: precursor films in the wetting of dry solids. *C. R. Acad. Sci. II* **299**, 499–503.
HOCKING, L.M. 1983 The spreading of a thin drop by gravity and capillarity. *Q. J. Mech. Appl. Math.* **36** (1), 55–69.
HOCKING, L.M. 1992 Rival contact-angle models and the spreading of drops. *J. Fluid Mech.* **239**, 671–681.
HOCKING, L.M. 1994 The spreading of drops with intermolecular forces. *Phys. Fluids* **6** (10), 3224–3228.
HOCKING, L.M. & RIVERS, A.D. 1982 The spreading of a drop by capillary action. *J. Fluid Mech.* **121**, 425–442.
HOFFMAN, R.L. 1975 A study of the advancing interface. I. Interface shape in liquid-gas systems. *J. Colloid Interface Sci.* **50** (2), 228–241.
HUH, C. & SCRIVEN, L.E. 1971 Hydrodynamic model of steady movement of a solid/liquid/fluid contact line. *J. Colloid Interface Sci.* **35** (1), 85–101.
HUPPERT, H.E. 1982 The propagation of two-dimensional and axisymmetric viscous gravity currents over a rigid horizontal surface. *J. Fluid Mech.* **121**, 43–58.
HUPPERT, H.E. 2006 Gravity currents: a personal perspective. *J. Fluid Mech.* **554**, 299–322.
JOANNY, J.F. & DE GENNES, P.G. 1986 Upward creep of a wetting fluid: a scaling analysis. *J. Phys. France* **47** (1), 121–127.
LOPEZ, J., MILLER, C. & RUCKENSTEIN, E. 1976 Spreading kinetics of liquid drops on solids. *J. Colloid Interface Sci.* **56** (3), 460–468.
LUO, J. & GAO, P. 2025 Explicit theory of moving contact lines. *J. Fluid Mech.* **1019**, A52.
MARSH, J.A., GAROFF, S. & DUSSAN V., E.B. 1993 Dynamic contact angles and hydrodynamics near a moving contact line. *Phys. Rev. Lett.* **70** (18), 2778–2781.
MCHALE, G., NEWTON, M.I., ROWAN, S.M. & BANERJEE, M. 1995 The spreading of small viscous stripes of oil. *J. Phys. D: Appl. Phys.* **28** (9), 1925.
NGAN, C. & DUSSAN V., E.B. 1982 On the nature of the dynamic contact angle: an experimental study. *J. Fluid Mech.* **118**, 27–40.
OTSU, N. 1979 A threshold selection method from gray-level histograms. *IEEE Trans. Syst. Man Cybernet.* **9** (1), 62–66.
PETROV, P. & PETROV, I. 1992 A combined molecular-hydrodynamic approach to wetting kinetics. *Langmuir* **8** (7), 1762–1767.
POPESCU, M., OSHANIN, G., DIETRICH, S. & CAZABAT, A. 2012 Precursor films in wetting phenomena. *J. Phys.: Condens. Matter* **24** (24), 243102.
RAMÉ, E. & GAROFF, S. 1996 Microscopic and macroscopic dynamic interface shapes and the interpretation of dynamic contact angles. *J. Colloid Interface Sci.* **177** (1), 234–244.
DE RUIJTER, M.J., DE CONINCK, J., BLAKE, T.D., CLARKE, A. & RANKIN, A. 1997 Contact angle relaxation during the spreading of partially wetting drops. *Langmuir* **13** (26), 7293–7298.

https://doi.org/10.1017/jfm.2026.11664 Published online by Cambridge University Press

DE RUIJTER, M.J., DE CONINCK, J. & OSHANIN, G. 1999 Droplet spreading: partial wetting regime revisited. *Langmuir* **15** (6), 2209–2216.

SIMPSON, J.E. 1999 Gravity currents: in the environment and the laboratory. In *Environment and the Laboratory*, vol. 79. Cambridge University Press.

SNOEIJER, J.H. 2006 Free-surface flows with large slopes: beyond lubrication theory. *Phys. Fluids* **18**, 021701.

STAROV, V.M., KOSTVINTSEV, S.R., SOBOLEV, V.D., VELARDE, M.G. & ZHDANOV, S.A. 2002*a* Spreading of liquid drops over dry porous layers: complete wetting case. *J. Colloid Interface Sci.* **252** (2), 397–408.

STAROV, V.M., KOSVINTSEV, S.R., SOBOLEV, V.D., VELARDE, M.G. & ZHDANOV, S.A. 2002*b* Spreading of liquid drops over saturated porous layers. *J. Colloid Interface Sci.* **246** (2), 372–379.

STAROV, V.M., ZHDANOV, S.A., KOSVINTSEV, S.R., SOBOLEV, V.D. & VELARDE, M.G. 2003 Spreading of liquid drops over porous substrates. *Adv. Colloid Interface* **104** (1), 123–158.

STAROV, V.M., ZHDANOV, S.A. & VELARDE, M.G. 2002*c* Spreading of liquid drops over thick porous layers: complete wetting case. *Langmuir* **18**, 9744–9750.

TANNER, L.H. 1979 The spreading of silicone oil drops on horizontal surfaces. *J. Phys. D: Appl. Phys.* **12** (9), 1473.

UNGARISH, M. 2009 *An Introduction to Gravity Currents and Intrusions*. CRC Press.

VOINOV, O.V. 1976 Hydrodynamics of wetting. *Fluid Dyn.* **11** (5), 714–721.

VOINOV, O.V. 1995 Spreading of a drop of viscous liquid over a surface under the action of capillary forces. *J. Appl. Math. Mech.* **59** (5), 735–743.

VOINOV, O.V. 1999 Gravity-induced spreading of a drop of a viscous fluid over a surface. *J. Appl. Mech. Tech. Phys.* **40** (3), 412–419.

WASHBURN, E.W. 1921 The dynamics of capillary flow. *Phys. Rev.* **17**, 273–283.

WHITAKER, S. 1986 Flow in porous media I: a theoretical derivation of Darcy's law. *Transp. Porous Med.* **1** (1), 3–25.

https://doi.org/10.1017/jfm.2026.11664 Published online by Cambridge University Press